

Composite to tilted vortex lattice transition in $\text{Bi}_2\text{Sr}_2\text{CaCu}_2\text{O}_{8+\delta}$ in oblique fields

M. Konczykowski^a, C.J. van der Beek^a, A.E. Koshelev^b, V. Mosser^c, M. Dodgson^d, and P.H. Kes^e

^a *Laboratoire des Solides Irradiés, CNRS-UMR 7642 & CEA/DSM/DRECAM, Ecole Polytechnique, Palaiseau, France*

^b *Materials Science Division, Argonne National Laboratory, Argonne, IL 60439, U.S.A.*

^c *ITRON, 50 Avenue Jean Jaurès, F-92120 Montrouge, France*

^d *Department of Physics and Astronomy, University College, Gower Street, London WC1E 6BT, U.K. and*

^e *Kamerlingh Onnes Laboratory, Leiden University, PO Box 9506, 2300RA Leiden, the Netherlands*

(Dated: March 19, 2007)

Precision measurements of the vortex phase diagram in single crystals of the layered superconductor $\text{Bi}_2\text{Sr}_2\text{CaCu}_2\text{O}_{8+\delta}$ in oblique magnetic fields confirm the existence of a second phase transition, in addition to the usual first order vortex lattice melting line $H_m(T)$. The transition has a strong first order character, is accompanied by strong hysteresis, and intersects the melting line in a tricritical point $(H_m^\perp, H_{cr}^\parallel)$. Its field dependence and the changing character of the melting line at the tricritical point strongly suggest that the ground state for magnetic fields closely aligned with the superconducting layers is a lattice of uniformly tilted vortex lines.

PACS numbers: 74.25.Qt, 74.25.Op, 74.25.Dw

The first order “vortex melting” transition from a solid (phase-ordered) state to a liquid state with only short range correlations is the main feature of the phase diagram of vortex lines in clean, layered high-temperature superconductors [1]. The application of a small field component H^\parallel , parallel to the superconducting layers, leads to a lattice of tilted vortex lines that melts in a similar fashion [2]. However, in the more anisotropic (layered) compounds such as $\text{Bi}_2\text{Sr}_2\text{CaCu}_2\text{O}_{8+\delta}$, the depression of the perpendicular component of the melting field H_m^\perp by larger parallel fields was interpreted as the consequence of the decomposition of the tilted vortex lattice into a combined lattice structure of Josephson Vortices (JVs) and Abrikosov-type pancake vortices (PVs) [2]. For very small field components H^\perp perpendicular to the layers, chain structures [3] arising from the attractive interaction of PVs with JVs were directly visualized by Bitter decoration [4, 5], scanning Hall-probe [3, 6] and magneto-optical techniques [7, 8]. At higher $H^\perp \sim H_m^\perp$, the contribution of the JVs to the free energy of the pancake vortex crystal results in the almost linear depression of H_m^\perp as function of the parallel field [2, 10, 11, 12]. This behavior in moderate H^\parallel stops at a temperature dependent characteristic field H_{cr}^\parallel . Even though melting is still observed above H_{cr}^\parallel , the variation of H_m^\perp with increasing H^\parallel becomes much weaker [11, 12]. Several controversial interpretations of this changing behavior were proposed, such as layer decoupling [11], a commensurate transition [13], and a matching effect [14].

In this Letter we focus on the high-temperature portion of the vortex phase diagram in single crystalline $\text{Bi}_2\text{Sr}_2\text{CaCu}_2\text{O}_{8+\delta}$ in oblique fields, which can be established precisely using the well-defined discontinuity of the vortex density at the melting transition. We show that $(H_m^\perp, H_{cr}^\parallel)$ corresponds to a tricritical point in the vortex lattice phase diagram, where the melting crosses a novel transition from a composite lattice at low parallel fields,

to another tilted lattice structure at *high* H^\parallel . The experimental observation of large hysteresis suggests that this transition is strongly first order, consistent with recent predictions [15]. The identification of the vortex ground state at high parallel field as a tilted lattice structure resolves the open problem of the apparent anisotropy factor γ_{eff} , and allows one to determine the enhancement of H_m^\perp by magnetic coupling. We find the temperature dependence of γ_{eff} to be consistent with previous observations [16, 17] and in quantitative agreement with the proposed model.

Experiments were performed on rectangular samples cut from $\text{Bi}_2\text{Sr}_2\text{CaCu}_2\text{O}_{8+\delta}$ single crystals with different oxygen content [18]. The c -axis component of the local magnetic induction $B^\perp(\mathbf{r})$ was measured by micro-Hall sensors placed on the central part of the sample. The 2D electron gas Hall sensors were fabricated in GaAlAs heterostructures and had $8 \times 8 \mu\text{m}^2$ active area. Results are presented in Fig. 1(a) as the local magnetization $H_s^\perp \equiv B^\perp - H^\perp$. The local dc magnetization of all crystals shows a sharp discontinuity, ΔB^\perp , at the vortex melting transition, that was tracked as function of H^\parallel at various fixed temperatures. The angle θ between the magnetic field and the crystalline c -axis was computer-controlled with 0.001° resolution, while the field magnitude could be swept up to 1 T using an electromagnet. Two types of magnetization loops were measured. In the first, the magnetization is traced as function of the c -axis field at constant H^\parallel ; in the second, the magnetization is measured as function of H^\parallel at constant H^\perp .

While the discontinuity in the dc magnetization gives a clear identification of the melting field, another method [19], in which the magnitude $B(f, T)$ of the periodic part of the induction above the sample is measured at the frequency f of an ac ripple field applied perpendicularly to the sample plane, is more convenient and precise. The ac response is represented as the transmittivity T' , *i.e.*

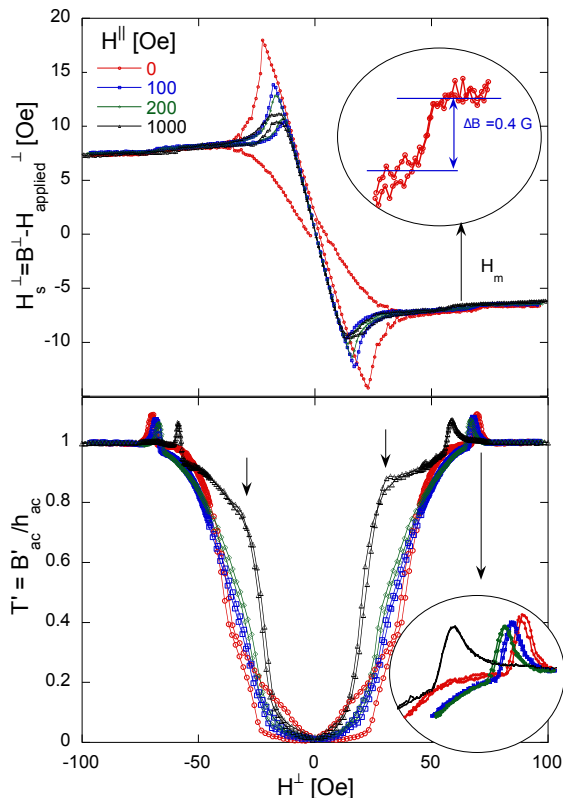


FIG. 1: (a) *dc* local magnetization loops recorded on an as-grown $\text{Bi}_2\text{Sr}_2\text{CaCu}_2\text{O}_{8+\delta}$ single crystal ($T_c = 88$ K) at 75 K, as function of the magnetic field component H^\perp perpendicular to the superconducting layers, with the in-plane field H_\parallel held constant. The inset shows a magnified view of the discontinuity at the vortex melting transition in $H_\parallel = 0$. (b) the in-phase (screening) component of the *ac* response of the same crystal, recorded under the same conditions, with an *ac* magnetic field of amplitude $h_{ac} = 0.8$ Oe and frequency $f = 11$ Hz applied along the *c*-axis. The melting transition shows up as a paramagnetic peak (see inset), the transition from combined to tilted vortex lattice is indicated by arrows. The *ac* response is plotted as the transmittivity $T' \equiv [B'(f, T) - B(f, T \ll T_c)]/[B(f, T > T_c) - B(f, T \ll T_c)]$.

the in-phase component $B'(f, T)$, normalized by the amplitude h_{ac} of the *ac* ripple [21]. The steplike feature in the *dc* magnetization loop at H_m^\perp translates to a paramagnetic peak in the *ac* response, shown in Fig. 1(b) [19]. The magnitude of this peak depends on the ratio of ΔB^\perp to h_{ac} . The peak position is independent of both the amplitude and frequency of the *ac* ripple. In the explored temperature range (above 50 K) and at low frequency (below 27 Hz), a true paramagnetic signal is measured. At higher frequencies or lower temperatures, flux pinning results in the partial shielding of the *ac* field [20]. Nevertheless, a peak-like feature persists at melting.

Figure 1(a) shows that at $T > 50$ K, the application of even a small magnetic field component parallel to the layers results in the drastic suppression of magnetic irre-

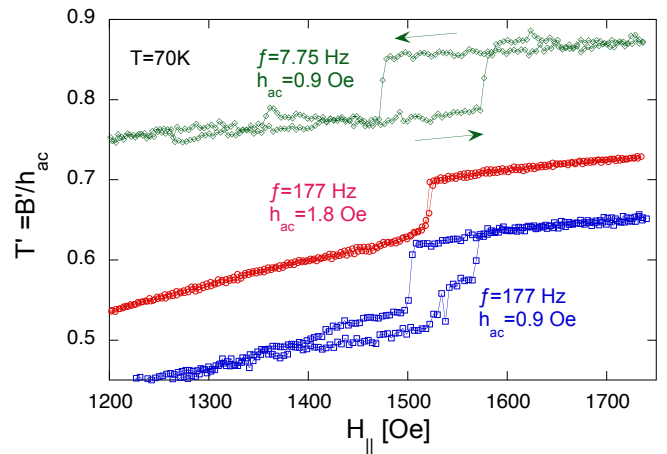


FIG. 2: Transmittivity T' of the same crystal as in Fig. 1, recorded at $T = 70$ K and constant $H^\perp = 58$ Oe, as a function of H_\parallel for various frequencies f and amplitudes h_{ac} of the *ac* ripple field. A marked hysteresis of the *ac* screening is observed. This hysteresis disappears when h_{ac} is increased.

versibility. This is expected when the geometric barrier is at the origin of flux pinning [22, 23]. Simultaneously, H_m^\perp is depressed linearly with increasing H_\parallel . However, at a well-defined value H_{cr}^\parallel , the dependence of H_m^\perp on in-plane field changes to a much slower, quadratic behavior that very well fits the anisotropic London model, $H_m(\theta) = H_{m0}/(\cos^2\theta + \sin^2\theta/\gamma_{eff}^2)^{1/2}$ [24]; *i.e.* the perpendicular component of the melting field

$$H_m^\perp = \sqrt{H_{m0}^{\perp 2} - \frac{H_\parallel^2}{\gamma_{eff}^2}} \approx H_{m0}^\perp \left(1 - \frac{H_\parallel^2}{2\gamma_{eff}^2 H_{m0}^{\perp 2}} \right). \quad (1)$$

The characteristic field H_{m0} and the effective anisotropy parameter γ_{eff} will be defined below.

In Fig. 1(b), another feature in the in-phase component of the *ac* response can be distinguished, at perpendicular fields H^\perp somewhat smaller than H_m^\perp . This feature is brought out much more clearly in sweeps of the parallel field, shown in Fig. 2. There is an abrupt jump from lower to higher values of T' on increasing H_\parallel , that only appears for parallel fields $H_\parallel \lesssim H_{cr}^\parallel$. The position of the jump does not depend on *ac* frequency. At low amplitude of the *ac* field, a pronounced hysteresis of T' is observed; this disappears if h_{ac} is sufficiently increased.

The transmittivity T' is simply related to the magnitude of the shielding current flowing in the sample in response to the applied *ac* magnetic field, a higher T' corresponding to a smaller current and less screening [21]. In the present case, *dc* magnetization loops point to the geometrical barrier [22] as the main source of screening. However, increasing the *ac* field frequency reduces the role of thermally activated depinning of vortices in the crystal bulk; as a consequence, a bulk screening current

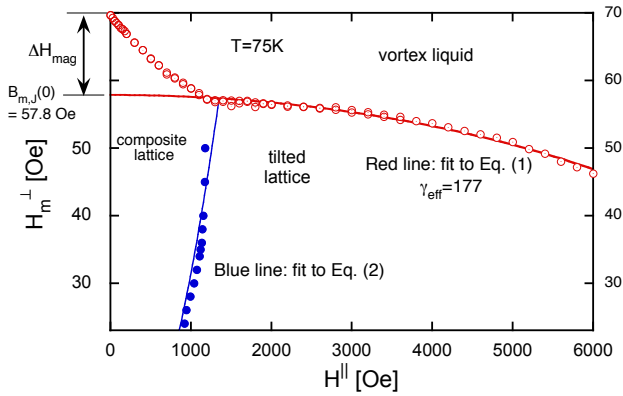


FIG. 3: Two field-component vortex-lattice phase diagram, with the first-order melting transition H_m^\perp (○) determined from the paramagnetic peak in T' , and the first-order transition to the tilted PV lattice at B_t (●), determined from the “glitch” in T' (Fig. 1 b). The dashed line is a fit to the composite-to-tilted lattice transition, Eq. (2) with $C = 0.030$; the continuous line is a fit of the high-field portion of the vortex lattice melting line to Eq. (1).

due to vortex pinning emerges [20]. At the frequencies of Fig. 2, the step in T' is due to a discontinuous change of the magnitude of this bulk current at the well-defined in-plane field, $H^\parallel \equiv H_{ct}^\parallel$. The location of H_{ct}^\parallel does not depend on the frequency and h_{ac} which indicates a *vortex phase transition in the bulk*, from a low H^\parallel -phase with higher pinning, to a high H^\parallel -phase with lower pinning. The hysteresis of the screening current indicates it to be first order.

In Fig. 3 we collect, for $T = 75$ K, the positions of the two first order transitions in a plot of H^\perp versus H^\parallel . The usual melting field H_m^\perp of the vortices, deduced from the paramagnetic peak in the transmittivity, shows the well-known linear decrease as function of H^\parallel [2, 10, 11, 12], up to the field component H_{cr}^\parallel . The field H_{ct}^\perp of the first order transition revealed by the (irreversible) transmittivity rapidly increases with H^\parallel and crosses the melting line at H_{cr}^\parallel in a tricritical point. The same scenario is observed at all explored temperatures ($T > 50$ K), with temperature dependent values of H_{cr}^\parallel . The anisotropy factor γ_{eff} , extracted from the London model fit to the high- H^\parallel part of the melting line, depends on temperature as well as on the oxygen content of the $\text{Bi}_2\text{Sr}_2\text{CaCu}_2\text{O}_{8+\delta}$ crystals; it is depicted in Fig 4.

The low- H^\parallel portion of the phase diagram with almost linear $H_m^\perp(H^\parallel)$ dependence has been interpreted as the region of crossing vortex lattices of JVs and PV stacks [2]. A more accurate analysis shows that other “composite-lattice” configurations compete for the ground state in the parameter range of $\text{Bi}_2\text{Sr}_2\text{CaCu}_2\text{O}_{8+\delta}$. These are the soliton lattice [25], as well as the set of combined lattices composed of regularly spaced rows of *tilted* pancake

stacks, separated by M rows of pancake stacks aligned with the c -axis. The latter type of lattice becomes favorable at smaller anisotropies and larger H^\parallel . Moreover, if H^\parallel is sufficiently large and the material anisotropy is not extremely high, a *simple* tilted lattice ($M = 0$) turns out to be the most favorable configuration. We interpret the experimentally observed transition as that from a composite to such a uniformly tilted lattice. A simple estimate for the in-plane field at which this transition is expected, B_{ct}^\parallel , can be obtained by comparing the ground state energies of the simplest ($M = 1$) composite lattice and of the uniformly tilted lattice, giving [15]

$$B_{ct}^\parallel \approx C \frac{\gamma}{\lambda_{ab}} \left[B^\perp \Phi_0 / \ln \left(\frac{1.55 \sqrt{B^\perp \Phi_0}}{s B_{ct}^\parallel} \right) \right]^{1/2}. \quad (2)$$

Here Φ_0 is the flux quantum, λ_{ab} is the ab -plane penetration depth, γ is the penetration depth ratio λ_c/λ_{ab} , and s is the layer spacing. Eq. (2) gives a very good fit to the experimental transition line, as illustrated in Fig. 3.

The anisotropic three-dimensional behavior (1) of H_m^\perp for large in-plane field $B^\parallel > B_{cr}^\parallel$ strongly supports this interpretation. The $H_m^\perp(H^\parallel)$ -dependence is the direct consequence of the vanishing contribution of the magnetic interaction between PVs to the vortex tilt stiffness in a highly inclined tilted vortex structure. The angular dependence of the melting field can be derived using a scaling transformation of coordinates, $\tilde{z} = \gamma^{2/3} z$; $\tilde{r}_\perp = \gamma^{-1/3} r_\perp$, which reduces the larger part of the free energy to an isotropic form [24]. In scaled coordinates the magnetic field is given by $\tilde{B} = B \gamma^{2/3} (\cos^2 \theta + \sin^2 \theta / \gamma^2)^{1/2}$, while the tilt angle $\tan \tilde{\theta} = \tan \theta / \gamma$. The Josephson tilt energy of a deformed vortex line (PV stack) in scaled coordinates,

$$E_{J,t} = \int \frac{d\tilde{k}_l}{2\pi} \frac{\tilde{\varepsilon}_1(\tilde{k}_l)}{2} \tilde{k}_l^2 |\delta \tilde{\mathbf{u}}(\tilde{k}_l)|^2,$$

is determined by the effective line tension $\tilde{\varepsilon}_1(\tilde{k}_l) = \tilde{\varepsilon}_0 \ln(1/\tilde{r}_{\text{cut}} \tilde{k}_l)$, valid when the wave vector along the line direction, \tilde{k}_l , is much larger than the vortex lattice zone boundary vector. Here, $\delta \tilde{\mathbf{u}}(\tilde{k}_l)$ is the Fourier transform of the line deformation, and $\tilde{\varepsilon}_0 = \varepsilon_0 \gamma^{-2/3}$ with $\varepsilon_0 \equiv \Phi_0^2 / (4\pi \lambda_{ab})^2$. For near-perpendicular fields ($\tilde{\theta} \ll 1$) the core cut-off distance \tilde{r}_{cut} is determined by the so-called thermal vortex wandering length, $\tilde{r}_{\text{cut}} \approx \langle \tilde{\mathbf{u}}_{n,n+1}^2 \rangle^{1/2} \equiv \langle (\tilde{\mathbf{u}}_{n+1} - \tilde{\mathbf{u}}_n)^2 \rangle^{1/2}$, where $\tilde{\mathbf{u}}_n$ is the position of the PV vortex in layer n [26]. For a *tilted* vortex line, $\tilde{\mathbf{u}}_{n,n+1} = s \tan \tilde{\theta} + \delta \tilde{\mathbf{u}}_{n,n+1}$ consists of the average displacement as well as random (thermal) fluctuations meaning that the core cut-off $\tilde{r}_{\text{cut}}^2 \approx s^2 \tan^2 \tilde{\theta} + \langle (\delta \tilde{\mathbf{u}}_{n,n+1})^2 \rangle$. The melting temperature is given by $T_m = A \sqrt{\tilde{\varepsilon}_1(1/\tilde{a})} \tilde{\varepsilon}_0 \tilde{a}$, with $\tilde{a} \equiv (\Phi_0/\tilde{B})^{1/2}$ and $A \approx 0.1$ [27]. Returning to real coord-

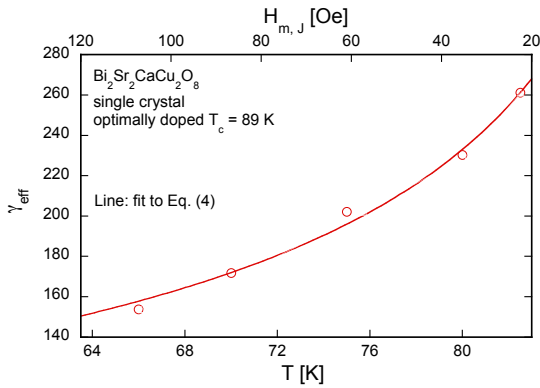


FIG. 4: Temperature dependence of the apparent anisotropy γ_{eff} extracted from the fits of the melting line to Eq. (1). The drawn line shows a fit to Eq. (4) with intrinsic $\gamma = 500$.

dinates, we obtain

$$T_m^2 = A^2(\epsilon_0 s)^2 \ln \left(\frac{C_J B_{sc}(\theta)/B}{r_0^2 + \tan^2 \theta / \gamma^2} \right) \frac{B_{sc}(\theta)}{B} \quad (3)$$

where the numerical constant $C_J \approx 5$ can be estimated within the self-consistent harmonic approximation, $B_{sc}(\theta) = (\Phi_0/\gamma^2 s^2)/\sqrt{\cos^2 \theta + \gamma^{-2} \sin^2 \theta}$, and $r_0^2 = \langle (\delta \mathbf{u}_{n,n+1})^2 \rangle / (\gamma s)^2 \approx 2A[\Phi_0/s^2 \gamma^2 B_m(0)]^{1/2}$. Note that the angular-dependent core cutoff introduces an additional angular dependence of melting field: T_m no longer depends only on the ratio $B_{sc}(\theta)/B$. In particular, a new angular scale appears given by $\tan \theta = \gamma r_0$. In the experimental angular range $\tan \theta \ll \gamma, \gamma r_0$, we recover Eq. (1) with the apparent anisotropy

$$\gamma_{eff} \approx \gamma \left(1 + \frac{10\sqrt{B_m(0)\gamma^2 s^2 / \Phi_0}}{\ln \left[\frac{68\sqrt{\Phi_0 / (B_m(0)\gamma^2 s^2)}}{1} \right]} \right)^{-1/2}. \quad (4)$$

We note several key points. First, the effective anisotropy γ_{eff} is manifestly smaller than the intrinsic γ . It increases with temperature, and is in excellent agreement with the experimental data of Fig.4, strongly suggesting that the modified core cut-off length originating from the tilting of the PV stacks determines the behavior of the melting line at high parallel fields. Very similar behavior has been observed in $\text{YBa}_2\text{Cu}_3\text{O}_{7-\delta}$ [16]. Next, the prefactor $H_{m0}^\perp = B_m(0)/\mu_0$ in Eq. (1) is to be interpreted as the hypothetical vortex melting field $H_{m,J}(\theta = 0)$ in the *absence* of the magnetic coupling between PVs. The difference $\Delta H_{mag} = H_m^\perp(\theta = 0) - H_{m,J}(0) \approx 0.15 H_m^\perp$ between the real (experimental) melting field and this prefactor represents the (remarkably modest) enhancement of the melting field due to magnetic coupling.

Summarizing, we have established the existence of phase transition of the vortex lattice in single crystalline $\text{Bi}_2\text{Sr}_2\text{CaCu}_2\text{O}_{8+\delta}$ in oblique fields. The transition has

a strong first order character and intersects the usual first order vortex lattice melting line at a tricritical point $[H_m^\perp(T), H_{ct}^\parallel(T)]$. For fields parallel to the superconducting layers $H^\parallel < H_{cr}^\parallel$ the melting line shows the signature of a composite lattice. For $H^\parallel > H_{cr}^\parallel$, the melting line is fully consistent with that of a uniformly tilted lattice of PV stacks. We thus propose that the new first order transition takes place between the combined and the tilted vortex lattice. For low in-plane fields, the combined vortex lattice is stabilized by the magnetic interaction between PV's in the same stack (vortex line). The enhancement of the melting line in the combined lattice regime is due to the contribution of this magnetic interaction to the vortex line tilt stiffness.

-
- [1] E. Zeldov *et al.*, Nature **375**, 373 (1995)
 - [2] A. E. Koshelev, Phys. Rev. Lett. **83**, 187 (1999).
 - [3] S. Bending and M. J. W. Dodgson, J. Phys.: Condens. Matter **17**, R955 (2005).
 - [4] C. A. Bolle, P. L. Gammel, D. G. Grier, C. A. Murray, D. J. Bishop, D.B. Mitzi, and A. Kapitulnik, Phys. Rev. Lett. **66**, 112 (1991).
 - [5] I. V. Grigorieva, J. W. Steeds, G. Balakrishnan, and D. M. Paul, Phys. Rev. B **51**, 3765 (1995).
 - [6] A. Grigorenko, S. Bending, T. Tamegai, S. Ooi, and M. Henini, Nature **414**, 728 (2001).
 - [7] V. K. Vlasko-Vlasov, A. Koshelev, U. Welp, G. W. Crabtree, and K. Kadowaki, Phys. Rev. B **66**, 014523 (2002).
 - [8] M. Tokunaga, M. Kobayashi, Y. Tokunaga, and T. Tamegai, Phys. Rev. B **66**, 060507 (R) (2002).
 - [9] B. Schmidt, M. Konczykowski, N. Morozov, and E. Zeldov, Phys. Rev. B **55**, R8705 (1997).
 - [10] S. Ooi, T. Shibauchi, N. Okuda, and T. Tamegai, Phys. Rev. Lett. **82**, 4308 (1999).
 - [11] M. Konczykowski, C. J. van der Beek, M. V. Indenbom, E. Zeldov, Physica C, **341**, 1213 (2000).
 - [12] J. Mirkovic, S. E. Savel'ev, E. Sugahara, and K. Kadowaki, Phys. Rev. Lett. **86**, 886 (2001).
 - [13] S. E. Savel'ev, J. Mirkovic, K. Kadowaki, Phys. Rev. B **64**, 094521 (2001).
 - [14] M. Tokunaga, M. Kishi, N. Kameda, K. Itaka, and T. Tamegai, Phys. Rev. B **66**, 220501(R) (2002).
 - [15] A.E. Koshelev, unpublished.
 - [16] A. Schilling, M. Willemin, C. Rossel, H. Keller, R.A. Fisher, N.E. Phillips, U. Welp, W.K. Kwok, R.J. Olsson, and G.W. Crabtree, Phys. Rev. B **61**, 3592 (2000).
 - [17] J. Mirković, S.E. Savel'ev, E. Sugahara, and K. Kadowaki, Phys. Rev. B **66**, 132505 (2002).
 - [18] M. Li, C.J. van der Beek, M. Konczykowski, A.A. Menovsky, and P.H. Kes, Phys. Rev. B **66**, 024502 (2002).
 - [19] N. Morozov, E. Zeldov, D. Majer, and M. Konczykowski, Phys. Rev. B **54**, R3784 (1996).
 - [20] M.V. Indenbom, C.J. van der Beek, V. Berseth, M. Konczykowski, N. Motohira, H. Berger and W. Benoit, J. Low Temp. Phys., **105**, 1117 (1996).
 - [21] J. Gilchrist and M. Konczykowski, Physica C **212**, 43 (1993).
 - [22] E. Zeldov, A.I. Larkin, V.B. Geshkenbein, M. Kon-

- czykowski, D. Majer, B. Khaykovich, V.M. Vinokur, and H. Shtrikman, Phys. Rev. Lett. **73**, 1428 (1994).
- [23] N. Morozov, E. Zeldov, M.Konczykowski, and R. A. Doyle, Physica C **291**, 113 (1997).
- [24] G. Blatter, V.B. Geshkenbein, and A.I. Larkin, Phys. Rev. Lett. **68**, 875 (1992).
12,14 (1964)
- [25] A.E. Koshelev, Phys. Rev. **68**, 094520 (2003).
- [26] A.E. Koshelev and V.M. Vinokur, Phys. Rev. B **57**, 8026 (1998); T.R. Goldin and B. Horovitz, Phys. Rev. B **58**, 9524 (1998).
- [27] A.E. Koshelev, H. Nordborg, Phys.Rev. **59**, 4358 (1999).